Inviscid-Viscous Interaction in Transonic Flows about Finite Three-Dimensional Wings

W. Kordulla*
NASA Ames Research Center, Moffett Field, Calif.

In order to include viscous effects, the inviscid small-disturbance solution of Bailey and Ballhaus for three-dimensional transonic flows has been combined with a finite-difference solution for Prandtl's boundary-layer equations. This solution employs the conditionally stable, implicit Krause scheme to cope with the domain-of-dependence problem for reverse cross flow. To be consistent with the inviscid-flow solution, the boundary layer is computed in the representative wing planform plane, which is transformed into rectangular shape in the computational domain. The flow has been assumed turbulent, and a scalar eddy viscosity model is adopted. The interaction between inviscid and viscous flow is modeled with the displacement surface, which is added to the geometric wing shape. Sample distributions of displacement thickness for swept wings are presented for weak and strong interaction cases. The displacement concept is shown to work for weak interaction on a nonlifting rectangular wing. The strong interaction on the ONERA M6 wing at an angle of attack of 3 deg can only be handled if the nonconservative method is used for the inviscid flow. The use of the correct fully conservative method needs further investigations with respect to the modeling of shock boundary-layer interaction and separation.

Introduction

CONVENTIONALLY, the design of transonic wings is based on many hours of expensive wind-tunnel tests. The overall cost of development can, however, be reduced considerably if comparatively cheap theoretical methods can be used in conducting parametric studies of the wing performance before a model is built and finally tested in the wind tunnel. It is, therefore, highly desirable to develop reliable and efficient methods to predict the transonic flowfield about three-dimensional (3-D) wings.

Recent literature[1-5] has shown that, in many cases, inviscid theory alone can be used to efficiently predict transonic flowfields about 3-D finite wings with reasonable accuracy. In some cases, however, the poor agreement between predicted and measured pressure distributions points to the importance of viscous effects such as shock wave boundary-layer interaction, trailing edge separation, and wake curvature. The appropriate means for predicting these effects, the solution of the Navier-Stokes equations, has been quite successful for two-dimensional airfoils in spite of crude turbulence modeling.[6] However, due mainly to the lack of sufficient computer power, there is no such solution available for 3-D wing configurations. A less costly alternative is to correct the inviscid solution for viscous effects by combining it with a boundary-layer solution via the displacement surface. Although recent investigations have shown that an accurate prediction of the inviscid-viscous interaction in the immediate neighborhood of shocks and the trailing edge requires a sophisticated three-layer modeling of the flow,[7,8] combined inviscid boundary-layer solutions have been successful in two dimensions[9-11] for high Reynolds number flows where the critical regions in question are sufficiently small to be neglected.

The present work extends the coupling of inviscid and boundary-layer solutions to 3-D transonic flows about finite wings, where a finite-difference solution for Prandtl's boundary-layer equations is coupled with the Bailey-Ballhaus small-disturbance relaxation method for the inviscid flow. Coupled inviscid boundary-layer solutions are also being developed at FFA and Dornier,[12] where an integral boundary-layer method[13] is being used. Although integral methods require less computation time than finite-difference methods, they present difficulties in defining appropriate profile families for reverse crossflow.[14] Finite-difference methods have no such difficulty and thus are preferred here.

To be consistent with small-disturbance theory, the boundary-layer computation is carried out in the planform plane of the wing, thereby neglecting curvature terms. This assumption is supported by the good agreement between predicted and experimental values of boundary-layer profiles and wall shear stress for infinite swept-wing flows when curvature terms are neglected in the governing equations.[15,16] For an incompressible laminar boundary layer on an uncambered wing, it has been shown[17] that neglecting curvature terms does not significantly change the solution away from the leading edge.

To be further consistent with the inviscid solution, the planform plane of a swept wing with finite tip is transformed into rectangular shape in the computational domain. The transformed boundary-layer equations are integrated with the conditionally stable Krause scheme.[18-20] This scheme has the advantage of maintaining the domain-of-dependence condition for reverse crossflow, without having to reorient the difference molecule when the spanwise flow changes direction. The Krause scheme has been applied successfully by different users for the computation of 3-D boundary layers on, for example, blunt bodies,[21] in the stagnation point region of blunted cones,[22] on pointed cones,[23] and on spinning cones[24] at angle of attack.

Following its successful application by others[9-11] in two dimensions, the 3-D displacement surface is assumed to couple the boundary layer and inviscid flow regions with sufficient accuracy. The displacement surface itself is obtained from a partial differential equation involving integral boundary-layer parameters. The modeling of the inviscid-viscous interaction is applied here only to the flow over the wing surface. The treatment of the wing wake, with its in-

Presented as Paper 77-209 at the AIAA 15th Aerospace Sciences Meeting, Los Angeles, Calif., Jan. 24-26, 1977; submitted March 3, 1977; revision received Dec. 13, 1977.

Index categories: Boundary Layers and Convective Heat Transfer—Turbulent; Jets, Wakes, and Viscid-Inviscid Flow Interactions; Transonic Flow.

*NRC Research Associate; presently DFVLR-Institut für Angewandte Gasdynamik, Köln, West Germany. Member AIAA.

fluence on lift for attached flows, is postponed to later work.

For the results presented in this paper, it is assumed that the boundary layer is fully turbulent everywhere, with the Reynolds stresses approximated by Cebeci's scalar eddy viscosity model. Due to the thin layer near the leading edge, however, the flow is practically laminar at that point. As the subject of transition is still being investigated,[25] no attempt has been made to examine the influence of the location of transition regions. Furthermore, recent measurements of transition on swept wings at angle of attack[26] show that the commonly made assumption of transition occurring along a line of constant chord is suspect.

After a discussion of the boundary-layer equations, the finite-difference solution, and the procedures involved in the inviscid-viscous interaction, examples of displacement thickness distributions for lifting and nonlifting flows about swept wings are given. Finally, the influence of viscous effects on the predicted pressure distribution is shown for the nonlifting flow about a rectangular wing and for the flow about a swept wing at an angle of attack of 3 deg.

Boundary-Layer Equations

The boundary layers developing on isolated wings, except in the immediate neighborhood of the tip, are of the boundary-sheet type, where viscous diffusion is considered only in the direction normal to the wall. Prandtl's boundary-layer equations in Cartesian coordinates are valid if the curvature of the surface is assumed small everywhere compared to the boundary-layer thickness. This is valid except close to the leading edge,[17] where the curvature of a wing surface is largest.

The transformation of the wing planform into rectangular shape in the computational domain introduces nonorthogonal coordinates, which are lines of constant chord and constant span (Fig. 1). The transformation is[1]

$$\xi=[x-x_{LE}(y)]c^{-1}(y) \qquad x=\xi c(\eta)+x_{LE}(\eta)$$

$$\eta=y \qquad y=\eta$$

$$\zeta=z \qquad z=\zeta \tag{1}$$

where c is the local chord length. The angle between the new coordinates (see Fig. 1) is given by the relation

$$\cos\theta=x_\eta(x_\eta^2+y_\eta^2)^{-1/2} \tag{2}$$

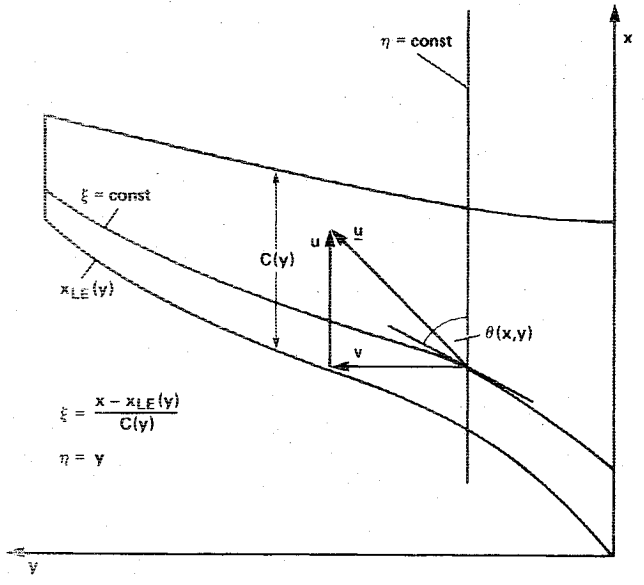

Fig. 1 Planform view of an isolated wing.

Only the independent variables are transformed in the boundary-layer equations.

Straightforward use of Eqs. (1) and (2) leads to the new set of governing equations with

$$\xi_y=-\xi_x x_\eta=-c^{-1}\cot\theta$$

Continuity:

$$c^{-1}[(\rho u)_\xi-\cot\theta(\rho v)_\xi]+(\rho v)_\eta+(\rho w)_\zeta=0 \tag{3a}$$

x-momentum:

$$Lu+c^{-1}p_\xi=0 \tag{3b}$$

y-momentum:

$$Lv+p_\eta-c^{-1}\cot\theta p_\xi=0 \tag{3c}$$

Energy:

$$LT-(k-1)[uc^{-1}p_\xi+v(p_\eta-c^{-1}\cot\theta p_\xi)]/k$$
$$-\mu(k-1)M_\infty^2[(u_\zeta)^2+(v_\zeta)^2]=0 \tag{3d}$$

where

$$L\equiv c^{-1}\rho(u-v\cot\theta)\frac{\partial}{\partial\xi}+\rho v\frac{\partial}{\partial\eta}+[\rho w-(\alpha\mu)_\zeta]\frac{\partial}{\partial\zeta}-\alpha\mu\frac{\partial^2}{\partial\zeta^2}$$

and $\alpha=Pr^{-1}$ for the energy equation and $\alpha=1$ otherwise.

Equations (3) describe turbulent flows in terms of time-averaged mean quantities. All variables are made nondimensional with freestream values and with the chord length c_R of the wing root. Stretching with the square root of the freestream Reynolds number is applied to the coordinate and velocity component normal to the wall. Pr is the Prandtl number and, for convenience, is set constant for laminar as well as turbulent flows (here, 0.85). The isentropic exponent k is the ratio of specific heats for thermally perfect gases. It is also assumed that the gas is calorically perfect.

In laminar flows, Sutherland's viscosity law is adopted. In turbulent flows, the scalar eddy viscosity model of Cebeci[27,28] is assumed to approximate the Reynolds number stressed with sufficient accuracy. Although it is well known that velocity gradient and shear stress are not collateral,[29,30] the eddy viscosity is taken independent of the direction. More sophisticated turbulence closures could be incorporated, but they are still in the development stage.

Adiabatic and isentropic relations are used to compute temperature and pressure from the velocity components supplied by the inviscid solution. This can be shown to be an exact solution of Eqs. (3) at the edge of the boundary layer. The wall boundary conditions are Stokes' no-slip condition and an adiabatic wall.

The definition of initial conditions completes the mathematical formulation. As with most 3-D boundary-layer methods, initial data are required in two planes. For isolated wings with a symmetry plane ($\eta=0$), quite accurate conditions can be prescribed in the planes $\eta=0$ and $\xi=0$, and also at the stagnation point $\eta=\xi=0$ (Fig. 1). Consistent with small perturbation theory, the stagnation plane is assumed to coincide with the plane $\zeta=0$. The equations that yield the initial conditions are derived from Eqs. (3) by taking their limit for $\eta\to0$ or $\xi\to0$ or both (symmetry plane and stagnation point equations).

Finite-Difference Solution of the Boundary-Layer Equations

The finite-difference methods for turbulent boundary layers encounter the problem of a rapidly increasing domain

of integration related to the growth of the boundary layer in the streamwise direction. Before integrating the boundary-layer equations, therefore, one may consider a transformation that gives an approximately constant domain of integration normal to the wall, in spite of the fast-growing turbulent boundary layer. Cebeci et al.[31] and Blottner,[32] for example, recommend the similarity-type transformation which is very efficient for laminar flows, because the value of the transformed wall-normal coordinate at the boundary-layer edge remains approximately constant. For turbulent flow, this value increases rapidly[32] and a highly nonuniform mesh with large geometric progression is neeeded to keep the number of points in a reasonable range. Nash and Scruggs,[33] on the other hand, use physical variables and scale the wall-normal coordinates with some function of the boundary-layer thickness. The present boundary-layer solution has not incorporated a particular scaling, other than with the square root of the Reynolds number, and uses a nonuniform mesh with geometric progression.

Finite-difference solutions for boundary-layer equations in three dimensions have to take special care of the domian-of-dependence condition.[17-20,32,34,35] A method formulated implicitly in the direction normal to the wall and marching pointwise in the spanwise direction is not stable and accurate unless it is upwind-oriented with respect to the crossflow. For this reason, the second-order accurate Keller box scheme used by Cebeci et al.[31] must be reoriented when negative crossflow is encountered. In principle, this reorientation problem disappears only when the solution is fully implicit in the spanwise plane. In their first-order accurate, alternating-direction-implicit scheme for the spanwise integration, Nash and Scruggs[33] improve stability by using upwind differencing for the spanwise and also wall-normal first derivative.

Here, the finite-difference solution of the boundary-layer equations is based on that of Krause[36] and Krause et al.[37] The advantage of the implicit Krause scheme[18] consists of its ability to march pointwise with conditional stability against crossflow.[18,21-24] With the exception of the spanwise derivative, the scheme (Fig. 2) involves Crank-Nicholson differencing. For Cartesian coordinates, Krause et al.[18] have demonstrated that the scheme can handle a change of flow angle of 135 deg across the boundary layer, if the step sizes in the directions parallel to the wall are equal. This feature, which also requires the prescription of only one initial condition for the spanwise integration, dominates the disadvantage that, at the end of the spanwise integration, some alternate technique has to be employed in order to prevent the domain of integration from shrinking when marching in the chordwise direction. Here, extrapolation has been used. A combination with respect to the extrapolated value of second-order extrapolations is preferred to a third-order extrapolation along lines of constant chord. Although a new, fully implict solution is currently under development, the pointwise marching Krause scheme is preferred for these initial interaction investigations because of the ease with which one can locally modify the inviscid boundary conditions for the boundary-layer solution, as necessary.

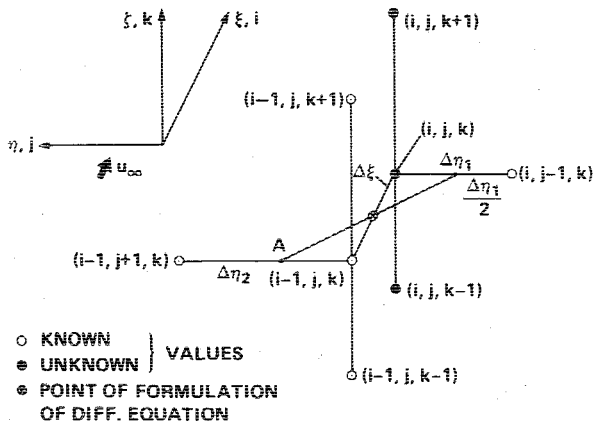

Fig. 2 Krause scheme in rectangular computational mesh.

A von Neumann stability analysis[38] for the linearized Eqs. (3) yields the condition[18]

$$v(u-v\cot\theta)^{-1}c\Delta\xi(\Delta\eta)^{-1}\geq -1 \tag{4}$$

Equation (4) insures stability if the domain-of-dependence condition is not violated.

For constant step sizes in the η and ζ directions, the Krause scheme is second-order accurate: $0[(\Delta\eta)^2+(c\Delta\xi)^2+(\Delta\zeta)^2]$. It is, however, desirable to use variable step sizes in order to reduce the computational effort. It is then known that second-order accurate discretization of second derivatives requires the difference of adjacent step sizes $(\Delta\zeta_2-\Delta\zeta_1)$ to be of the order of their product $\Delta\zeta_1\cdot\Delta\zeta_2$. The finite-difference approximation of the first η-derivative shows a similar pattern. If one chooses to approximate the η-derivative at the point $(i-1/2, j, k)$ in Fig. 2 by the average of the η-derivatives at $(i, j-1/2, k)$ and at point A in Fig. 2, then an error $0(\Delta\eta_2-\Delta\eta_1)$ follows, due to the two-point interpolation of the values at point A.

The verification of numerical techniques by comparing solutions with experimental data is important. Unfortunately, no boundary-layer investigation data on 3-D transonic finite wings are available.[14] In addition, when different theoretical techniques are compared, care must be taken that the external boundary conditions are the same. An arrangement such as the Trondheim trials,[39] which compared different prediction methods for incompressible turbulent infinite swept-wing flows, would be of great use with respect to code testing.

As the field calculation of the present method is based on the code written and tested in 1968 for laminar flows,[18,37] and because other authors[21-24] have demonstrated the correctness and applicability of the scheme for laminar and turbulent flows, a check of the entirely new parts which concern the initial conditions would have been sufficient. The stagnation-point solution has been checked against Libby's theoretical data,[40] and the two-dimensional solution for the initial conditions has been compared with experimental data for two-dimensional flows about subcritical[41] and supercritical[42] airfoils. Changes in the organization of the code, however, required further checks for the field calculation. Due to the lack of established experimental and theoretical data for 3-D transonic wings, three checks have been performed. One used the solution obtained with the ordinary rectangular 4-point scheme[37] to compare with. Another check was based on a quasi-two-dimensional solution with large, favorable pressure gradient. To enable a check, the axis had been turned by 45 deg, such that a fully 3-D problem with strong gradients in both tangential directions resulted. A final check was made by comparing solutions obtained from Eqs. (3) and from fully transformed equations[17,31] with curvature terms in the chordwise direction neglected. These comparisons ensured the correctness of the solution.

Procedure of Inviscid-Viscous Interaction

As mentioned earlier, the inviscid-viscous interaction is modeled by using the displacement surface, which reflects the influence of the wing boundary layer on the oncoming inviscid flow as new boundary condition for the inviscid-flow computation. Because it determines the external boundary conditions for the boundary-layer calculation, the new inviscid flowfield feeds the viscosity influence back to the boundary layer. This interaction concept results in an iterative procedure, which, for transonic flow, has global character due to the mixed elliptic-hyperbolic character of the inviscid equations.

Convergence of the interaction iterations is checked by comparing C_p values in the planes closest to the root and the

tip on lower and upper surface in successive iterations. In addition, integrated quantities such as lift, moment, and drag are checked. A relative change of typically 2% is assumed to indicate a converged solution. To avoid oscillations of C_p, the displacement surface introduced into the inviscid code is underrelaxed with a typical factor of 0.5.

The 3-D displacement thickness δ^* is well known to be the solution of a partial differential equation in contrast to mere quadrature in two dimensions.[40,43,44]

$$[(\rho u)_e(\delta^* - \delta_u^*)]_\xi + L[(\rho v)_e(\delta^* - \delta_v^*)] = 0 \qquad (5)$$

where $L = -\cot\theta\ \partial/\partial\xi + c\ \partial/\partial\eta$. Equation (5) is integrated using the Krause scheme after the boundary-layer profiles have been determined.

In cases with strong inviscid-viscous interaction, the boundary-layer solution may predict separation. The appropriate means to take care of this situation with boundary-layer equations is to define the region of separated flow and then to model the displacement surface in that region. In three dimensions, the definition of separated flow regions requires quite sophisticated programming and bookkeeping. Here, a simpler approach is chosen, where the external boundary conditions at each point are adjusted such that separation is circumvented. As soon as the chordwise wall shear stress turns negative, the velocity component u_e is increased by a certain percentage of the difference between its original value and the value one step ahead. Then, the chordwise integration step is repeated and the wall shear stress checked again. This procedure is repeated until the wall shear stress becomes positive. If the adjusted u_e value becomes larger than its value at one step ahead, the program stops.

The initial inviscid solution often causes the boundary layer to separate prematurely. One method for preventing the initial boundary layer from separating consists of smoothing the given u_e distribution before the boundary-layer integration is initiated. The smoothing consists of taking the average of u_e and of its value extrapolated from the two neighboring points. In the course of the inviscid-viscous iterations, the smoothing would be reduced and, if necessary, the adjusting procedure employed.

The Bailey-Ballhaus method used for the inviscid-flow prediction is available with either fully conservative (FCR) or nonconservative (NCR) relaxation. The conservative differencing insures that captured shock waves satisfy the shock conditions contained in the inviscid governing equation. This is not the case for nonconservative differencing. While FCR predicts shock waves that are too strong compared with experimental data, NCR coincidentally captures shock waves that are in better agreement with experimentally determined shock waves. Because the NCR method gives weaker shock strengths, it is sometimes advantageous to start on FCR boundary-layer combination cases with the NCR solution. Both FCR and NCR use scheme 3, explained in Ref. 3, which has been shown to better capture swept shocks.

Distribution of Displacement Thickness on Swept Wings

As the displacement thickness is the salient ingredient in the inviscid-viscous interaction model, some displacement thickness distributions are given for two supercritical flows about swept wings. One flow is an example for weak inviscid-viscous interaction, while the other flow is characterized by strong interaction. The inviscid flowfield is obtained by the NCR method, with the pressure calculated from both the chordwise and spanwise velocity components. This inviscid pressure formulation is consistent with the boundary-layer method, which uses the inviscid u and v velocity components to specify the external boundary conditions.

The boundary-layer method uses a computational mesh of $115 \times 23 \times 70$ (average value) for the first and of $130 \times 23 \times 75$ (average value) for the second flow in ξ, η, and ζ directions. Twenty percent of the chordwise points are employed on the first 5% chord. In comparison with the mesh used by Hirschel et al.[17] for laminar incompressible boundary layers on swept wings, the present mesh is chosen coarse. This was done because emphasis is put on the applicability of the displacement surface concept, and because the displacement thickness is fairly insensitive to small oscillations that may result from too large step sizes. The inviscid flowfield about the symmetric RAE 101 A wing at $M_\infty = 0.9$ and zero angle of attack poses no serious problem, such as separation to the boundary-layer method, because strong shocks are absent.

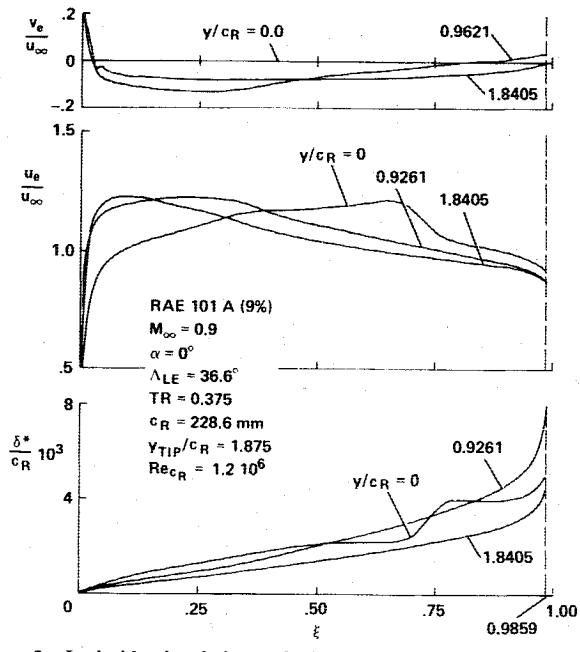

Fig. 3 Inviscid chordwise velocity distributions and predicted displacement thickness for the RAE wing.

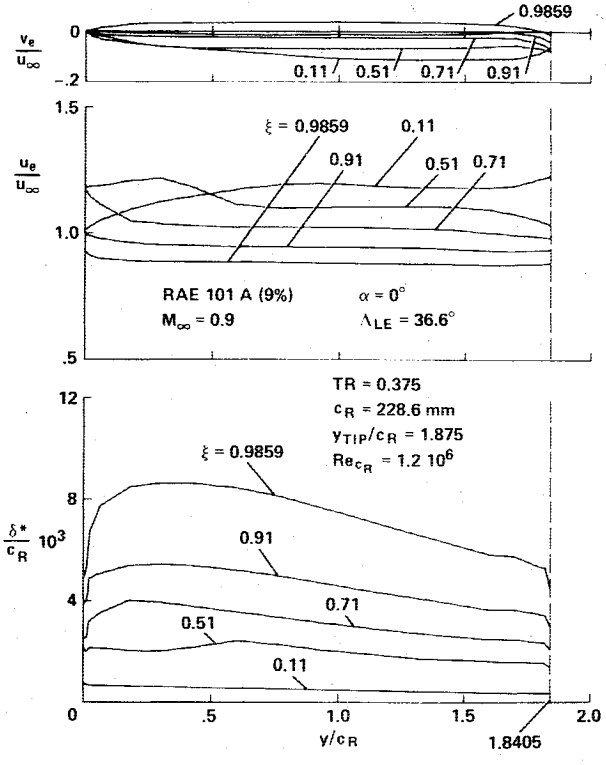

Fig. 4 Inviscid spanwise velocity distributions and predicted displacement thickness for the RAE wing.

Figures 3 and 4 present the variation of displacement thickness δ^* in chordwise and spanwise directions together with the Cartesian velocity components. The chordwise distribution of δ^* along $y=0$ exhibits the typically steep increase at the location of the weak shock (Fig. 3). Close to the trailing edge, δ^* increases further due to the recompression on the rear part of the wing. In the plane closest to the wing tip, the steep increase of velocity and the subsequent smooth recompression result in a moderate, nearly linear increase of δ^*. For $\xi=0.51$ and 0.71, steep decreases in spanwise direction of the chordwise velocity component u_e are noticed in Fig. 4. These decelerations correspond to the swept shock and generate increases of δ^*, such that a spanwise maximum of δ^* close to the plane $y=0$ develops with increasing ξ (Fig. 4). Away from the maxima, δ^* decreases smoothly in the direction of the tip, while the decrease toward the symmetry plane is rather steep.

Along $y=0$, δ^* develops a sharp minimum with increasing ξ, which can be explained as a three-dimensional effect caused by the variation of the spanwise gradient of the spanwise velocity component (flow divergence and convergence). Equation (5), which describes the change of δ^*, also allows negative values, which are quite unlikely to occur in attached two-dimensional boundary layers.

The assumption of locally infinite swept-wing conditions (for constant span, the correct boundary conditions are used while the η-derivatives in Eqs. (3) are neglected) along the tip or root is often used to generate initial conditions for the spanwise integration. The Krause scheme enables one to check these assumptions in the case of an isolated wing. The RAE 101 A wing, however, cannot be regarded as a severe test case because the spanwise convection and, therefore, the domains of influence, remain small.

The flow about the ONERA M 6 wing[45] at an angle of attack of 3 deg and for $M_\infty=0.92$ is more difficult to predict because strong swept shocks are present that induce separation. In addition, the spanwise component of the velocity is no longer small compared with the chordwise component, such that, near the tip on the upper surface, stability restrictions are imposed on the chordwise step size due to Eq. (4). A coarse mesh in the spanwise direction was adopted in order to avoid such stability restrictions. The fully implicit method, currently in development, will be free of this kind of restriction.

As mentioned earlier, smoothing or adjusting procedures are used to circumvent a breakdown of the boundary-layer calculation due to separation. Figure 5 presents chordwise distributions of u_e and v_e and corresponding δ^*. Approximations of u_e are shown that result from heavy smoothing over about the aft 60% chord of the wing, or from adjusting u_e. It is noted that the inviscid NCR solution employed a coarse mesh beyond 60% chord, which caused considerable smearing of the shock. Compared to the δ^* distributions for adjusted u_e values, the effect of heavy smoothing of u_e is less dramatic than expected close to the tip, while at mid-semispan, separation is prevented. The prediction still signals separation in the streamwise direction close to the tip, which is overcome by adjusting u_e adequately.

The regions of steepest increase in δ^* correspond to the locations of predicted separation. The solution along $y=0$ predicts negative values for δ^*, due to the variation of flow divergence and convergence inside the boundary layer in that symmetry plane. Stock[13] predicted negative δ^* close to the wing root for one case, too, using an integral method. The swept shock can at $\xi\approx0.6$ and 0.85 clearly be traced in the distributions of u_e and δ^*.

In contrast to the RAE wing calculations, the assumption of locally infinite swept-wing flow has a considerable effect on δ^* with respect to the finite-wing solution (Fig. 6). Close to the root, its influence is again restricted to a narrow region because of the small spanwise convection there. Due to large negative crossflow (Fig. 5), the regions of influence are wider close to the tip. Under infinite swept-wing conditions, no adjustments are necessary and separation is not predicted.

Results for the Inviscid-Viscous Interaction

Two transonic flow cases are investigated, one about a nonlifting rectangular wing and the other about a swept, lifting wing. The nonlifting flow about a rectangular wing (NACA 63 A006 profile) at $M_\infty=0.9$ and $Re_c=3\times10^6$ was investigated first, in order to check the displacement surface concept.

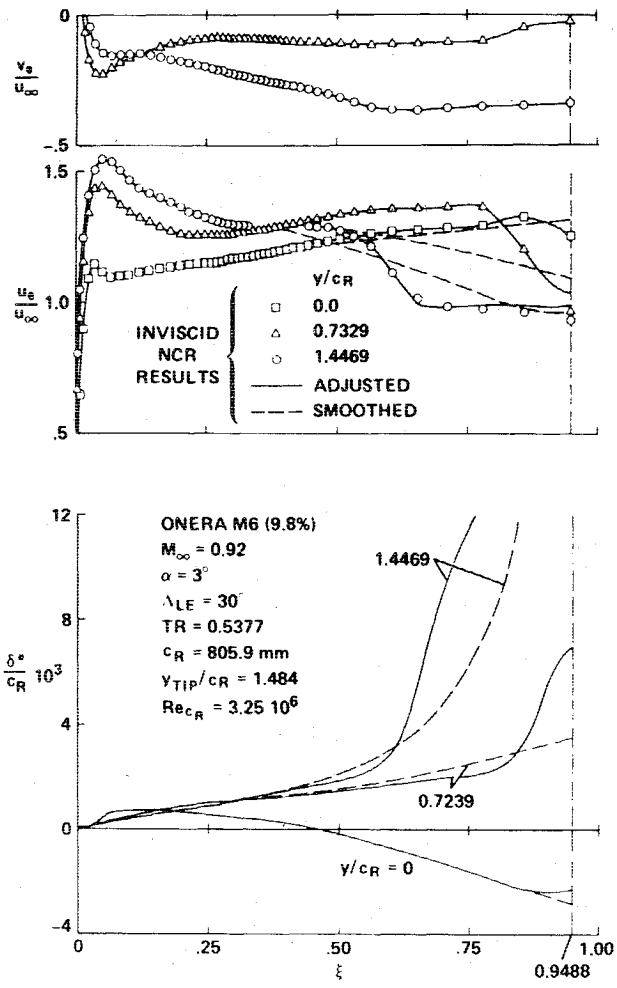

Fig. 5 Inviscid chordwise velocity distributions and predicted displacement thickness for the ONERA M 6 wing (upper surface).

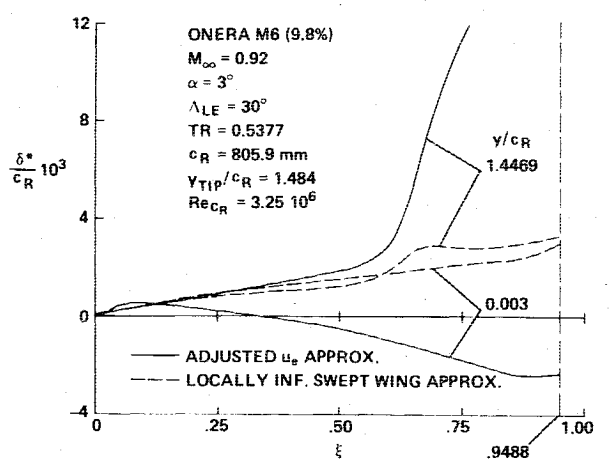

Fig. 6 Influence of locally infinite swept-wing assumptions on the displacement thickness for the ONERA M 6 wing (upper surface).

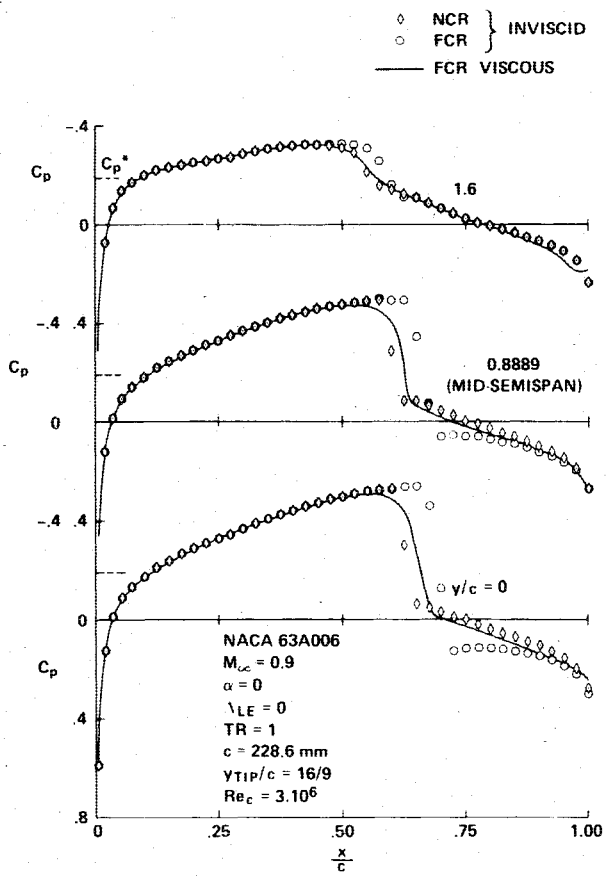

Fig. 7 Comparision of predicted inviscid and viscous C_p distributions for a rectangular wing.

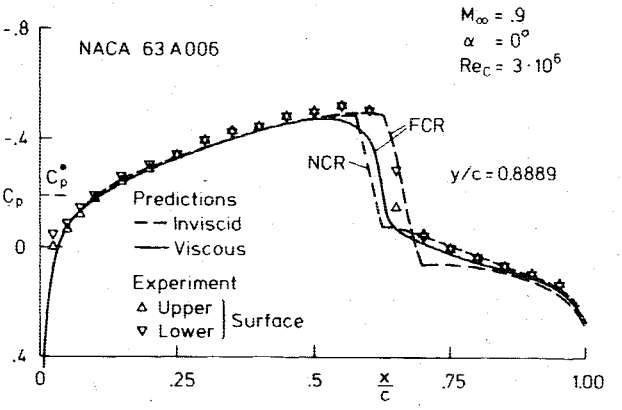

Fig. 8 Comparison of predicted and measured C_p distributions for a rectangular wing.

This flow is not strongly three-dimensional, because the maximum of the inviscid spanwise flow is roughly 6% of the freestream value and the shock is only slightly swept, but it does exhibit 3-D features such as reverse crossflow. Also, due to the tip and the swept shock, the isobars are not parallel to the leading edge. Figure 7 compares results of the purely inviscid NCR and FCR solutions with those obtained by the viscous FCR solution. Because of the viscous influence, the shocks predicted by the FCR method move upstream compared to the locations predicted by the purely inviscid FCR solution, and come close to the shock locations obtained with the purely inviscid NCR solution. It is encouraging to find the predicted pressure coefficients close to the NCR results because, in general, these happen to give better comparison with experiment. As expected, the displacement effect is felt only in the immediate neighborhood and aft of the shock wave. The interaction seems to be sufficiently weak to be captured by the displacement surface concept. Six iterations were needed to obtain convergence for a displacement relaxation factor of 0.5. Lower values of this factor increased the number of iterations.

Figure 8 compares predicted with measured C_p values for the mid-semispan station, where the influence of the fuselage, present in the experiment,[46] is negligible. The comparison is rather delicate (see also Ref. 1), because it is unusual that the commonly used NCR solution (the small-disturbance as well as the full-potential solution[1]) predict the shock location more upstream than observed in experiment. The complete reason is not well known. One reason is that the built wing has a shape sufficiently different from the exact NACA profile[47] used in the prediction. Another is indicated by Bailey and Ballhaus,[1] who estimate that the disagreement may be caused by the test Mach number being slightly higher than 0.90. Finally, the influence of the porous wind tunnel walls at that high Mach number is not well known. The trailing-edge comparison, however, is predicted very well with the NCR scheme. The fact that the inviscid FCR solution predicts a shock location fairly close to the experimental one, which is unfortunately only poorly defined, is meaningless because viscous effects are completely neglected. These are expected to move the inviscid shock upstream. This behavior is predicted by the viscous FCR solution, thereby approaching the results obtained with the NCR solution. In spite of the difficulties associated with the comparison in Fig. 8 it is therefore concluded that the displacement thickness concept is valid.

The second case, transonic lifting flow about a swept wing, is of more practical interest. Although the ONERA M 6 wing[45] is not a typical supercritical wing,[48] it has been chosen because of the large amount of numerical inviscid data available at Ames.

Figure 9 compares C_p distributions for this case as predicted by FCR and NCR methods with experimental data. Shock positions and strengths vary considerably, depending on whether NCR or FCR is used. The inviscid solutions retain, as mentioned earlier, additional terms in the governing equation (scheme 3 in Ref. 3) and have been shown to improve the capturing of swept shocks in the $M_\infty = 0.84$ flow case at the same angle of attack. Therefore, it is surprising that the weak shocks between 20 and 40% chord, shown in Fig. 9, are not predicted. A comparison calculation, performed with the Jameson[5] code, which solves the full potential equation in a nonconservative fashion, confirms the Ames' results. There are several possible causes for the disagreement; for example, dissipation or too coarse a grid in the inviscid method or the measured C_p values could be influenced by tunnel wall interference.

In order to avoid a breakdown of the viscous flow solution due to chordwise shock-induced separation when coupled directly with the FCR solution, the combined computation was first carried out with the NCR version. The global iteration started with the original inviscid results presented in Fig. 5. Although the boundary conditions for the viscous solution were initially smoothed even more than is shown in Fig. 5, the pressure distributions, obtained in the course of iteration cycles, induced separation on the aft portion of the wing. In addition to the smoothing and adjusting procedures described earlier, the displacement surface slopes had to be limited where separation was predicted, because the gradients near the trailing edge would otherwise be too steep and thus induce strong expansion in the inviscid solution instead of the measured recompression.

Figure 10 compares inviscid with viscous NCR predictions of C_p. An improvement in shock position and strength due to the addition of viscous effects can be seen on the upper surface. The situation on the lower surface can possibly be improved when the Kutta condition is replaced by an appropriate wake shape, thus influencing the lift. The displacement bump due to a shock moves the shock upstream

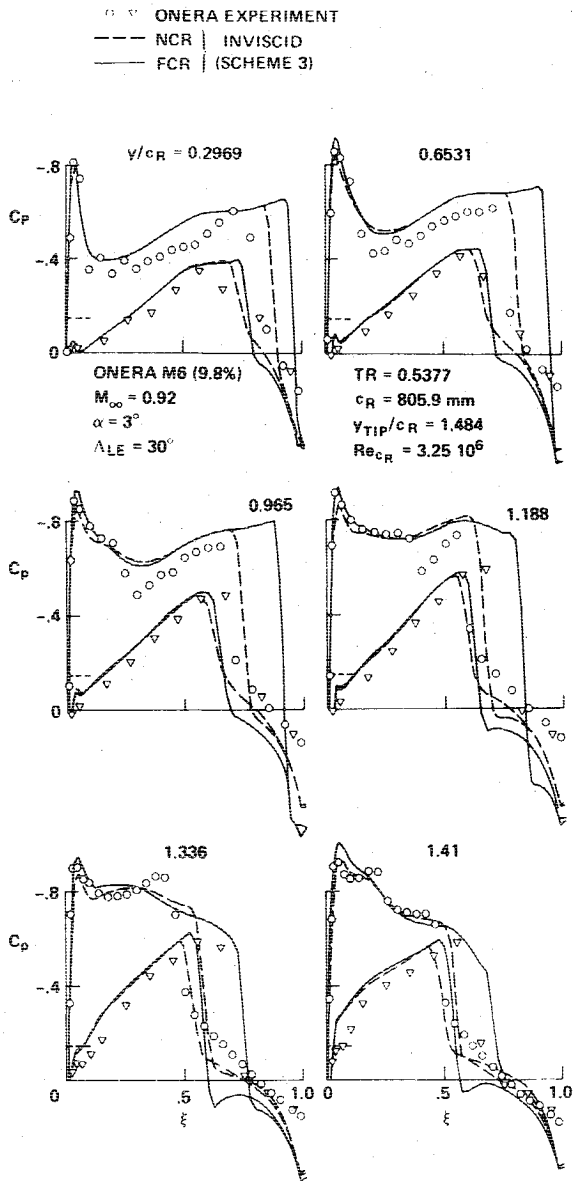

Fig. 9 Comparison of measured and predicted inviscid C_p distributions for the ONERA M 6 wing.

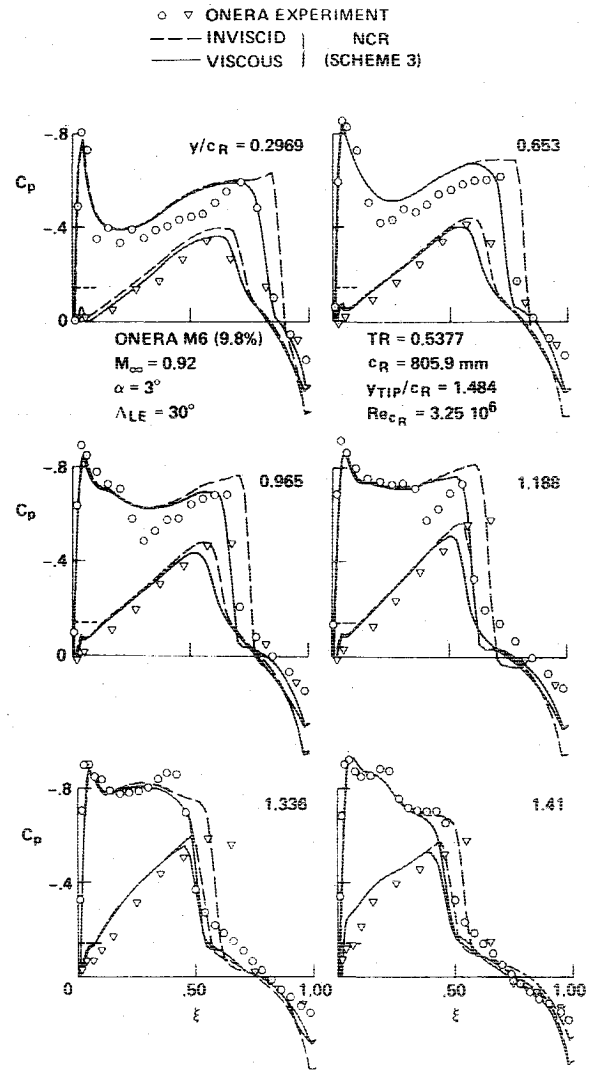

Fig. 10 Comparison of measured and predicted C_p distributions for the ONERA M 6 wing.

when incorporated as a fixed boundary condition for the inviscid flow. It may be more advantageous to introduce a viscous ramp, a wedge located at the base of the inviscid normal shock which converts the normal shock into an oblique shock with decreased shock strength.[49] In the inviscid solution, such a displacement ramp would be floating with the shock wave, thus allowing more freedom to move for the shock within the purely inviscid iterations. In this context, it is noted that it is necessary to start the NCR solution from scratch in order to make it unique. If, for example, the solution is initially based on converged FCR results, the NCR method will yield shocks that are too strong. The FCR solution, however, is considered unique.

The combined FCR boundary-layer solution started with the results presented in Fig. 10. Although the number of inviscid iterations between adding the displacement surface was kept low (50) to prevent the gradients from steepening too rapidly, it was rather discouraging to see the shocks moving away from experiment toward the converged inviscid location, resulting in a poor improvement over the purely inviscid solution. The interaction is obviously too strong to be modeled properly by the displacement surface concept the way it was done here.

Concluding Remarks

Initial results of a combined inviscid-viscous solution for transonic flows about 3-D isolated wings are presented. The improved inviscid small-disturbance solution of Bailey and Ballhaus[3] has been coupled to a pointwise marching, implicit finite-difference viscous solution that takes advantage of the Krause scheme to cope with the domain-of-dependence problem. This scheme allows one to check the commonly adopted assumption of locally infinite swept-wing flow to generate spanwise initial conditions. As expected, the error due to this assumption becomes largest close to the wing tip when large negative crossflow is present.

Sample distributions of displacement thickness are presented for the nonlifting flow about the RAE 101 A wing at $M_\infty = 0.9$ and the flow about the ONERA M 6 wing at an angle of attack of 3 deg for $M_\infty = 0.92$. For the case of predicted separation, the inviscid flow data are either smoothed or the main stream component is adjusted such that the calculation can just proceed.

For the nonlifting $M_\infty = 0.9$ flow about a rectangular wing with 6% NACA profile, it is shown that the combined FCR boundary-layer solution works. For the $M_\infty = 0.92$ flow about the ONERA M 6 wing at an angle of attack of 3 deg, reasonable results have been obtained for the combined NCR boundary-layer solution only. Although the viscous FCR solution used these results as initial conditions, the computed pressure distributions moved more and more toward the purely inviscid values and a poor improvement was obtained.

This suggests that more sophisticated modeling is needed for the displacement thickness in regions with separation; that is, for the case of strong interaction. The idea of a viscous ramp floating with the shock while incorporated in the inviscid FCR solution promises some relief for the shock boundary-layer problem, although it still needs more calibration. Where possible, future investigations should include the influence of the wake, as is done in several two-dimensional calculations.[11]

Acknowledgment

The author gratefully acknowledges the postdoctoral associateship at NASA Ames granted by the National Research Council. He is also indebted to E. Krause, Aerodynamisches Institut, West Germany, for helpful discussions, and to F. R. Bailey, W. F. Ballhaus, and J. Frick, NASA Ames Research Center, for their support with respect to the inviscid flow program.

References

[1] Bailey, F. R. and Ballhaus, W. F., "Comparisons of Computed and Experimental Pressures for Transonic Flows about Isolated Wings and Wing-Fuselage Configurations," NASA SP-347, 1975, pp. 1213-1231.

[2] Ballhaus, W. F., "Some Recent Progress in Transonic Flow Computations," VKI LS 87, 1976.

[3] Ballhaus, W. F., Bailey, F. R., and Frick, J., "Improved Computational Treatment of Transonic Flow about Swept Wings," *Advances in Engineering Science*, NASA CP-2001, Vol. 4, 1976.

[4] Bailey, F. R., "On the Computation of Two- and Three-Dimensional Steady Transonic Flows by Relaxation Methods," *Lecture Notes in Physics*, Vol. 41, Springer Verlag, New York, 1975, pp. 1-77.

[5] Jameson, A., "Transonic Flow Calculations," VKI LS 87, 1976.

[6] Deiwert, G. S., "Computation of Separated Transonic Turbulent Flows," *AIAA Journal*, Vol. 14, June 1976, pp. 735-740.

[7] Melnik, R. E. and Grossman, B., "Further Developments in an Analysis of the Interaction of a Weak Normal Shock Wave with a Turbulent Boundary Layer," *Symposium Transsonicum II*, Springer-Verlag, New York, 1976, pp. 262-272.

[8] Melnik, R. E. and Chow, R., "Asymptotic Theory of Two-Dimensional Trailing-Edge Flows," NASA SP-347, 1975, pp. 177-250.

[9] Bauer, F., Garabedian, P., Korn, D., and Jameson, A., "Supercritical Wing Sections II," *Lecture Notes in Economics and Mathematical Systems*, Vol. 108, Springer-Verlag, New York, 1975.

[10] Bavitz, P. C., "An Analysis Method for Two-Dimensional Transonic Viscous Flow," NASA TND-7718, 1975.

[11] Lock, R. C., "Research in the UK on Finite Difference Methods for Computing Steady Transonic Flows," *Symposium Transsonicum II*, Springer-Verlag, New York, 1976, pp. 457-486.

[12] Hedman, S. C., "Pressure Distributions for a Swept Wing Body Configuration Obtained from Coupling Transonic Potential Flow Calculations and Boundary Layer Calculations," AGARD Paper 18, CP 204, Feb. 1977.

[13] Stock, H. W., "Results of a Calculation Method for Three-Dimensional Compressible Turbulent Boundary Layers," Paper presented at the Federal Republic of Germany/USAF Data Exchange Agreement Meeting, Dayton, Ohio, April 1976.

[14] Johnston, J. P., "Experimental Sudies in Three-Dimensional Turbulent Boundary Layers," Report MD-34, Stanford University, Calif., July 1976.

[15] Krause, E., "Analysis of Viscous Flows over Swept Wings," *Proceedings of the 9th ICAS Congress*, Paper 74-20, Haifa, 1974.

[16] Adams, Jr., J. C., "Numerical Calculation of the Subsonic and Transonic Turbulent Boundary Layer on an Infinite Yawed Airfoil," AEDC TR 73-112, 1973.

[17] Hirschel, E. H., Jawtusch, V., and Grundmann, R., "Berechnung Dreidimensionaler Grenzschichten an Pfeilflügeln," Paper DGLR 76-187, presented at DGLR-Jahrestagung, München, Germany, Sept. 1976.

[18] Krause, E., Hirschel, E. H., and Bothmann, T., "Die Numerische Integration der Bewegungsgleichungen Dreidimensionaler Laminarer Kompressibler Grenzschichten," Fachtagung Aerodynamik, Berlin 1968, DGLR-Fachbuchreihe Band 3, Braunschweig, 1969.

[19] Krause, E., "Numerical Treatment of Boundary Layer Problems," AGARD LS 64, Feb. 1973.

[20] Krause, E., Hirschel, E. H., and Kordulla, W., "Fourth-Order Mehrstellen-Integration for Three-Dimensional Turbulent Boundary Layers," *Computers and Fluids*, Vol. 4, No. 2, 1976, pp. 77-92.

[21] Blottner, F. G. and Ellis, M. A., "Finite-Difference Solutions of the Incompressible Three-Dimensional Boundary Layer Equations for a Blunt Body," *Computers and Fluids*, Vol. 1, No. 2, 1973, pp. 133-158.

[22] Lin, T. C. and Rubin, S. G., "A Two-Layer Model for Coupled Three-Dimensional Viscous and Inviscid Flow Calculations," AIAA Paper 75-853, Hartford, Conn., June 1975.

[23] Harris, J. E., "An Implicit Finite-Difference Procedure for Solving the Three-Dimensional Compressible Laminar, Transitional and Turbulent Boundary Layer Equations," NASA SP-347, 1975.

[24] Watkins, Jr., C. B., "Numerical Solution of the Three-Dimensional Boundary Layer on a Spinning Sharp Body at Angle of Attack," *Computers and Fluids*, Vol. 1, No. 4, 1973, pp. 317-329.

[25] Hirschel, E. H., "The Influence of the Free-Stream Reynolds Number on Transition in the Boundary Layer on an Infinite Swept Wing," AGARD Report 602, 1972, pp. 1.1-1.11.

[26] Armand, C., "Etude de la Couche Limite par Détecteurs à Film Chaud en Ecoulement Subsonique et Transonique," *La Recherche Aérospatiale*, Annéé 1976, No. 3, May-June, pp. 127-133.

[27] Cebeci, T. and Smith, A. M. O., *Analysis of Turbulent Boundary Layers*, Academic Press, New York, 1974.

[28] Cebeci, T., "Calculation of Three-Dimensional Boundary Layers II. Three-Dimensional Flows in Cartesian Coordinates," *AIAA Journal*, Vol. 13, Aug. 1975, pp. 1056-1064.

[29] East, L. F., "Measurements of the Turbulent Boundary Layer on a Slender Wing," paper presented at the Euromech Colloquium 33, Three-Dimensional Turbulent Boundary Layers, Berlin, Sept. 1972.

[30] van den Berg, B., "Investigation of Three-Dimensional Incompressible Turbulent Boundary Layers," NLR TR 76001 U, 1976.

[31] Cebeci, T., Kaups, K., and Ramsey, J., "A General Method for Calculating Three-Dimensional Compressible Laminar and Turbulent Boundary Layers on Arbitrary Wings," Douglas Aircraft Company Rept. MDC J7267, 1976, (NASA CR-2777, 1977).

[32] Blottner, F. G., "Computational Techniques for Boundary Layers," AGARD LS 73, Feb. 1975.

[33] Nash, J. F. and Scruggs, R. M., "An Implicit Method for the Calculation of Three-Dimensional Boundary Layers on Fuselage Configurations," Lockheed Georgia Rept. LC 76 ER 0199, 1976.

[34] Wang, K. C., "On the Determination of the Zones of Influence and Dependence for Three-Dimensional Boundary Layer Equations," *Journal of Fluid Mechanics*, Vol. 48, Part 2, 1971, pp. 397-404.

[35] Kitchens, Jr., C. W., Sedney, R., and Gerber, N., "The Role of the Zone of Dependence Concept in Three-Dimensional Boundary-Layer Calculations," *Proceedings of AIAA 2nd Computational Fluid Dynamics Conference*, Hartford, Conn., June 1975, pp. 102-112.

[36] Krause, E., "Numerical Solutions of Boundary Layer Equations," *AIAA Journal*, Vol. 5, July 1967, pp. 1231-1237.

[37] Krause, E., Hirschel, E. H., and Bothmann, T., "Differenzenformeln zur Berechnung Dreidimensionaler Grenzschichten," DLR FB 69-66, 1969.

[38] Richtmyer, R. D. and Morton, K. W., *Difference Methods for Initial Value Problems*, 2nd ed., Interscience, New York, 1967.

[39] East, L. F., "Computation of Three-Dimensional Turbulent Boundary Layers," Euromech 60, Trondheim, FFA TN AE-1211, 1975.

[40] Libby, P. A., "Heat and Mass Transfer at a General Three-Dimensional Stagnation Point," *AIAA Journal*, Vol. 5, March 1967, pp. 507-517.

[41] Cook, T. A., "Measurements of the Boundary Layer and Wake of Two Aerofoil Sections at High Reynolds Numbers and High-Subsonic Mach Numbers," RAE TR 71127, 1971.

[42] Hurley, F. X., Spaid, F. W., Roos, F. W., Stivers, Jr., L. S., and Bandettini, A., "Detailed Transonic Flow Field Measurement about a Supercritical Airfoil Section," NASA TM X-3244, 1975.

[43] Moore, F. K., "Displacement Effect on a Three-Dimensional Boundary Layer," NACA Rept. 1124, 1953.

[44] Nash, J. F. and Patel, V. C., *Three-Dimensional Turbulent Boundary Layers*, SBC Technical Books, Atlanta, 1972.

[45] Monnerie, B. and Charpin, F., "Essais de Buffeting d'une Aile en Flèche Transonique," A.A.A.F., 10e Colloque D'Aérodynamique Appliqué, Lille, Nov. 1973.

[46] Binion Jr., T. W., "Investigation of Three-Dimensional Wall Interference in a Variable Porosity Transonic Wind Tunnel," AEDC TR 74-76, 1974.

[47] Ballhaus, W. F., private communication.

[48] Withcomb, R. T., "Advanced Transonic Aerodynamic Technology," *Advances in Engineering Science*, Vol. 4, NASA CP-2001, 1976, pp. 1521-1538.

[49] Magnus, R. and Yoshihara, H., "The Transonic Oscillating Flap," AIAA Paper 76-327, 1976.